arXiv:2306.12339v1 [cond-mat.mes-hall] 21 Jun 2023

Non-linear and negative effective diffusivity of optical excitations in moiré-free heterobilayers

Edith Wietek,[1] Matthias Florian,[2] Jonas M. Göser,[3] Takashi Taniguchi,[4] Kenji Watanabe,[5] Alexander Högele,[3,6] Mikhail M. Glazov,[7] Alexander Steinhoff,[8,9] and Alexey Chernikov[1,*]

[1] *Institute of Applied Physics and Würzburg-Dresden Cluster of Excellence ct.qmat, Technische Universität Dresden, 01062 Dresden, Germany*
[2] *University of Michigan, Department of Electrical Engineering and Computer Science, Ann Arbor, Michigan 48109, USA*
[3] *Fakultät für Physik, Munich Quantum Center, and Center for NanoScience (CeNS), Ludwig-Maximilians-Universität München, 80539 München, Germany*
[4] *Research Center for Materials Nanoarchitectonics, National Institute for Materials Science, 1-1 Namiki, Tsukuba 305-0044, Japan*
[5] *Research Center for Electronic and Optical Materials, National Institute for Materials Science, 1-1 Namiki, Tsukuba 305-0044, Japan*
[6] *Munich Center for Quantum Science and Technology (MCQST), 80799 München, Germany*
[7] *Ioffe Institute, 194021 Saint Petersburg, Russian Federation*
[8] *Institut für Theoretische Physik, Universität Bremen, 28334 Bremen, Germany*
[9] *Bremen Center for Computational Materials Science, Universität Bremen, 28334 Bremen, Germany*

Interlayer exciton diffusion is studied in atomically-reconstructed $MoSe_2/WSe_2$ heterobilayers with suppressed disorder. Local atomic registry is confirmed by characteristic optical absorption, circularly-polarized photoluminescence, and g-factor measurements. Using transient microscopy we observe propagation properties of interlayer excitons that are independent from trapping at moiré- or disorder-induced local potentials. Confirmed by characteristic temperature dependence for free particles, linear diffusion coefficients of interlayer excitons at liquid helium temperature and low excitation densities are almost 1000 times higher than in previous observations. We further show that exciton-exciton repulsion and annihilation contribute nearly equally to non-linear propagation by disentangling the two processes in the experiment and simulations. Finally, we demonstrate effective shrinking of the light-emission over time across several 100's of picoseconds at the transition from exciton- to the plasma-dominated regimes. Supported by microscopic calculations for bandgap renormalization to identify Mott threshold, this indicates transient crossing between rapidly expanding, short-lived electron-hole plasma and slower, long-lived exciton populations.

Within the rich family of van der Waals heterostructures [1, 2], artificially stacked bilayers of semiconducting transition metal dichalcogenides (TMDCs) emerged as a highly interesting platform for condensed matter research [3, 4]. They offer novel pathways to design electronic states by tuning local atomic registries through angular and lattice mismatch [5–11], revealing a plethora of many-body phenomena [12–14]. Importantly, electron-hole excitations in these systems are governed by strong Coulomb interaction, forming tightly-bound excitons [3, 15]. They often involve spatially-separated electron and hole constituents, conceptually similar to the excitons in coupled quantum wells [16, 17]. These interlayer excitons (IXs) can be long-lived [18], manipulated and guided by external fields [19], exhibit long valley-polarization lifetimes [20], and demonstrate correlated phenomena [14, 21]. They emerged as the main carriers of energy and quantum information in van der Waals heterostructures. Naturally, the question of how the excitons propagate attracted an increasing amount of attention, bridging the realms of optics and transport [20, 22–27] with promising pathways towards excitonic devices [19, 28].

Despite recent progress, however, it remains very challenging to disentangle intrinsic and extrinsic phenomena associated with van der Waals heterostructures that determine exciton transport. Primarily, these include trapping due to disorder from strain and dielectric effects [29] or within the moiré-induced potentials [5–11]. Both induce localization of excitons, evidenced by vanishing diffusion coefficients, observed at low temperatures [26, 27]. Moreover, exciton-exciton interactions lead to strongly non-linear effects, typically considered to stem from dipolar repulsion in analogy to coupled quantum wells [17, 24, 27, 28, 30, 31]. In contrast, exciton-exciton annihilation often determines effective diffusion in the monolayer constituents [32, 33]. Finally, the Mott transition from excitons to plasma already occurs at excitation densities of a few $10^{12}\,\mathrm{cm}^{-2}$ [21], leading to observations of rapid effective diffusion [27, 34]. To understand exciton propagation in van der Waals heterobilayers, the following questions thus need to be resolved: What are the pristine properties of propagating interlayer excitons *in the absence* of disorder and moiré potentials? Which non-linear effects are important and how can they be distinguished? Is there any *qualitative* impact of excitons and plasma on the propagation dynamics at the Mott transition?

Here, we address these questions by focusing on interlayer excitons in a prototypical heterobilayer systems,

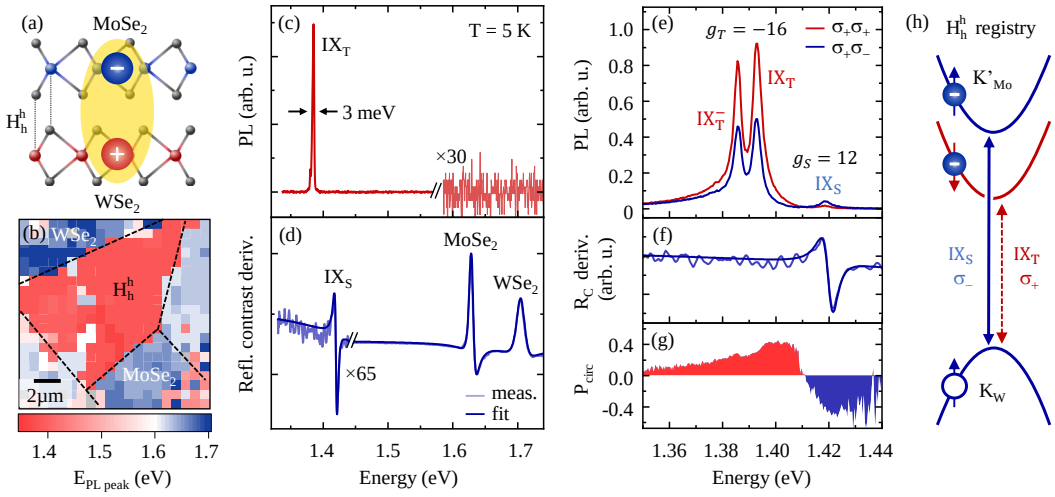

FIG. 1. (a) Schematic illustration of an interlayer exciton in a H_h^h reconstructed $MoSe_2/WSe_2$ heterobilayer. (b) PL peak energy map at T = 5 K. (c) Representative PL spectrum under low-density pumping. (d) Reflectance contrast derivative with fit from transfer matrix analysis. (e) Circularly polarized PL after σ_+-polarized, pulsed excitation with g-factors from magneto-optical measurements. (f) Reflectance contrast derivative, R_C, and (g) degree of circular polarization, $P_{circ} = (PL_+ - PL_-)/(PL_+ + PL_-)$. (h) Optical selection rules for H_h^h-stacked $MoSe_2/WSe_2$ heterobilayer (adapted from Ref. [35]).

$MoSe_2/WSe_2$, schematically illustrated in Fig 1. Taking advantage of the recently demonstrated conditions for atomic reconstruction [36–38], we realize the scenario of sufficiently large, moiré-free domains with fixed interlayer registry. The encapsulation in high-quality hBN suppresses extrinsic sources of disorder. Employing time-resolved optical microscopy, we find that interlayer excitons are highly mobile even at low densities and cryogenic temperatures. The measured diffusion coefficients are almost 1000 times higher than previously reported at comparable conditions [26, 27] in moiré systems. The absence of trapping is strongly supported by a characteristic temperature dependence for free propagation. Further, we disentangle two main sources of non-linear effective diffusion, demonstrating nearly equal contributions from exciton-exciton repulsion and annihilation. Finally, we show that propagation dynamics of optically induced excitations undergo a substantial change above the Mott transition. Most strikingly, it leads to the appearance of *negative* effective diffusion, indicating transient crossing between plasma- and exciton-dominated regimes.

The hBN-encapsulated $MoSe_2/WSe_2$ heterostructures were fabricated by mechanical exfoliation and dry viscoelastic transfer [39]. Matching angular alignment was confirmed by second-harmonic generation measurements, indicating H-type stacking; see Supplemental Material (SM). The samples were placed in a liquid-helium microscopy-cryostat and closed-cycle magneto-cryostats for transient diffusion and g-factor measurements, respectively. For photoluminescence (PL) studies we employed both continuous wave excitation (2.33 eV photon energy) and Ti:Sapphire laser (80 MHz repetition rate, 140 fs pulses), tuned to the photon energy of the $MoSe_2$ A-exciton of 1.63 eV. Reflectance measurements were performed using a tungsten halogen lamp. The signals were resolved spectrally and spatially by a grating and a mirror, respectively. They were detected either by a charged-coupled device or by a streak camera. Detailed description of the experimental setup is outlined in Refs. [32, 40] and SM.

As illustrated in Fig. 1 (b), the PL of the heterostructure region appears at photon energies around 1.4 eV at T = 5 K, as expected for IXs in $MoSe_2/WSe_2$ [18]. A typical spectrum at low-density, continuous-wave excitation is dominated by a single peak with 3 meV linewidth (Fig. 1 (c)). No emission from the intra-layer excitons is detected. The IX PL is accompanied by a sharp resonance in the reflectance contrast derivative spectrum, presented in Fig. 1 (c). Its oscillator strength is determined to be about 2% of the intra-layer excitons, consistent with Refs. [35, 41]. This implies good interlayer contact for sufficient electron-hole wavefunction overlap and the presence of atomic reconstruction. Most importantly, the reflectance contrast spectrum is a superposition of the individual $MoSe_2$ and WSe_2 monolayer spectra, slightly shifted and broadened. No resonance splitting and redistribution of the oscillator strengths are observed, demonstrating the absence of moiré potentials [8]. Circularly-polarized PL indicates emission from spin-singlets IX_S and spin-triplets IX_T with high and low oscillator strengths, respectively, presented in Figs. 1 (d)-(f). They correspond to the K_W-K'_{Mo} electronic transitions, consistent with the optical selection rules of H_h^h registry, illustrated in Fig. 1 (g) [35]. The lowest energy peak stems from IX_T^- trions [23, 42–44] due to weak non-intentional doping below 10^{11} cm^{-2}, as

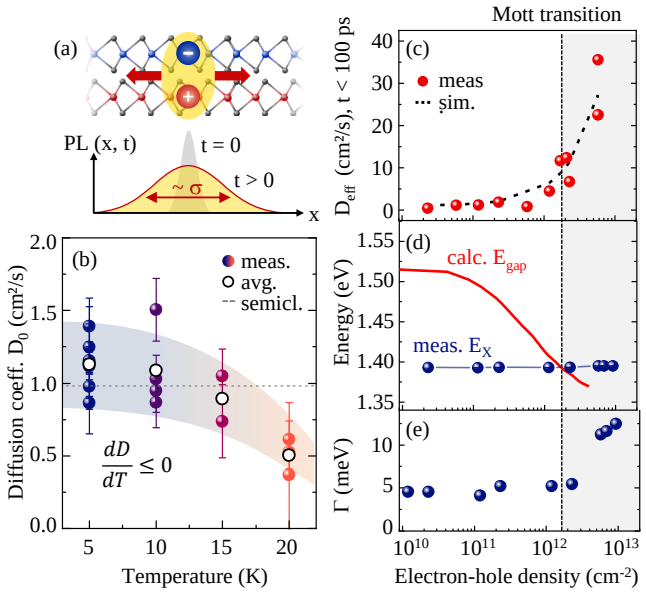

FIG. 2. (a) Schematic illustration of transient microscopy. (b) Temperature-dependent, linear diffusion coefficient D_0 at injection density of $1.2\times10^{11}\,\mathrm{cm}^{-2}$ electron-hole pairs per pulse (pump energy density: $0.5\,\mu\mathrm{J\,cm}^{-2}$). (c) Effective diffusion coefficients extracted during the first 100 ps after the excitation. (d) Calculated free particle bandgap, renormalized due to the presence of free charge carriers, and measured exciton peak energy. (e) Lineshape broadening at the Mott transition.

observed in gate-dependent measurements (see SM). Finally, both the absolute peak energies and the g-factors obtained from magneto-PL of $g_S = 12$ and $g_T = -16$ strongly support the H^h_h registry assignment in the sample [38, 45].

To demonstrate that IXs are free to move in the absence of moiré localization and disorder across a spatially-extended, reconstructed domain we perform time- and spatially-resolved exciton diffusion experiments, Fig. 2 (a), at low pump power and as a function of temperature. Measured, linear diffusion coefficients D_0, extracted within the IX lifetime below 1 ns (see SM), are presented in Fig. 2 (b). Notably, the average value of $1.1 \pm 0.2\,\mathrm{cm}^2/\mathrm{s}$ at $\mathrm{T} = 5\,\mathrm{K}$ is about 1000 times higher than previously found for moiré potentials at low densities [26, 27]. The diffusion matches the semi-classical expectation of $D_0 = 0.98\,\mathrm{cm}^2/\mathrm{s}$ using the scattering time obtained from the spectral broadening (see SM) and is decreasing with temperature. The physics of IX propagation in the heterostructure thus closely resemble those of $\mathrm{WSe_2}$ monolayers [46], with the 5 K diffusion being determined by the exciton-phonon interaction. Rapid diffusion of free IXs further rationalizes comparatively short lifetimes due to associated increase of the non-radiative capture probability [47].

Non-linear propagation is presented in Fig. 2 (c) as a function of optically injected electron-hole pair density n_{eh}. The effective diffusion coefficient, evaluated during the first 100 ps after the excitation, increases above $30\,\mathrm{cm}^2/\mathrm{s}$ at $n_{eh} = 6 \times 10^{12}\,\mathrm{cm}^{-2}$. This densities covers the Mott transition from excitons to electron-hole plasma, typically found in $\mathrm{MoSe_2/WSe_2}$ heterostructures in this range [21]. Using the theoretical approach from Refs. [21, 48], we determine the Mott threshold by calculating the renormalization of the quasiparticle bandgap as a function of electron-hole density (see SM) for the studied H^h_h registry. The assumptions of the model based on free carriers should be applicable close to the Mott transition. The absolute energy of the bandgap is fixed for the lowest densities to the sum of the exciton peak energy and the exciton binding energy. The latter was set to 130 meV in heterobilayers according to both calculated value and literature [15]. The Mott threshold is estimated from the crossing of the calculated bandgap and measured exciton peak energies, see Fig. 2 (d). The obtained value of $2 \times 10^{12}\,\mathrm{cm}^{-2}$ is consistent with literature [21], further supported by the onset of spectral broadening (Fig. 2 (e)).

The origin of the non-linear increase of the effective diffusion coefficient is commonly attributed to exciton-exciton *annihilation* (EEA) in monolayers [32, 33] and exciton-exciton *repulsion* in heterostructures [24, 27] and coupled quantum wells [49]. These two processes enter the diffusion equation as the last two terms in:

$$\frac{\partial n}{\partial t} = D_0 \Delta n - \frac{n}{\tau} - R_A n^2 + \frac{U_0 D_0}{k_B T} \nabla \cdot (n \nabla n), \qquad (1)$$

where D_0 and τ are the linear diffusion coefficient and exciton lifetime at low-densities, respectively, R_A the annihilation rate coefficient, U_0 the interaction constant ($U_0 n$ corresponds to the blue shift of the exciton peak), and k_B is the Boltzmann constant. We solve Eq. (1) numerically by using the initial shape of the excitation spot as a boundary condition, fixing D_0 and τ to the measured values, and varying R_A and U_0 parameters (see SM). The resulting changes of the mean-squared-displacement, $\Delta\sigma^2$, corresponding to the increase of the PL emission area over time [50], are presented in Fig. 3 (a) together with the measured data at selected densities. Interestingly, setting either R_A or U_0 strictly to zero demonstrates that neither the effective diffusivity $D_{\mathrm{eff}} \propto \partial\sigma^2/\partial t$ nor the $\Delta\sigma^2(t)$ traces identify the origin of the non-linear propagation.

To distinguish annihilation and repulsion, we consider relative increase of the spatially- and time-dependent PL instead, presented in Fig. 3 (b) as $\Delta\,\mathrm{PL} = [\mathrm{PL}(t) - \mathrm{PL}(0)]/\mathrm{PL}_{\mathrm{max}}$ from simulations. In the case of repulsion, the increase of the PL counts on the flanks of the excitation spot stem from the drift of the excitons towards outer regions. For annihilation only, the increase of $\Delta\,\mathrm{PL}$ stems exclusively from linear diffusion and is very small. Experimentally, changes in $\Delta\,\mathrm{PL}$ can be de-

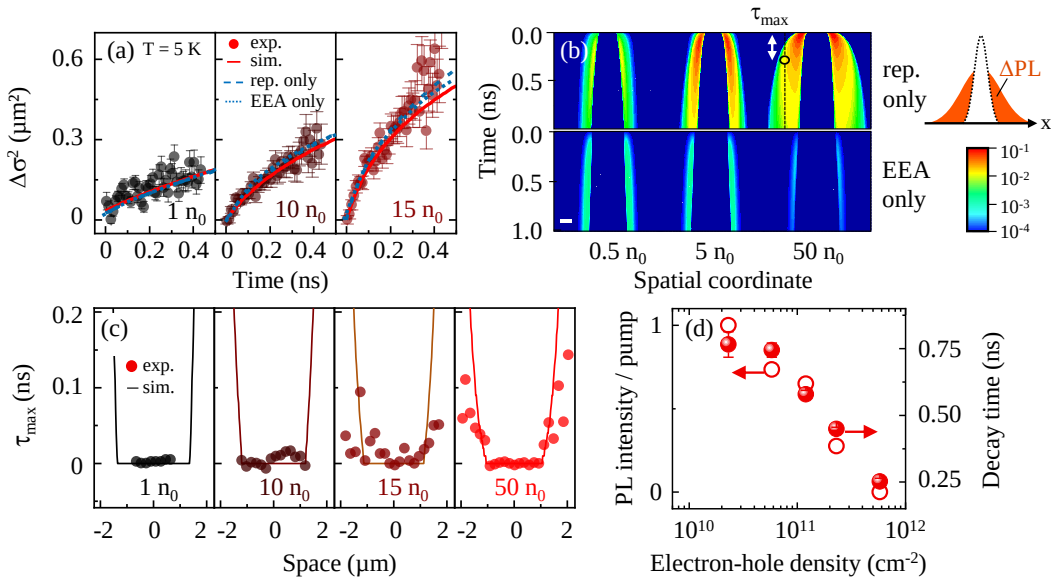

FIG. 3. (a) Mean squared displacement of IX for selected densities in units of $n_0 = 1.2 \times 10^{11}\,\mathrm{cm}^{-2}$. Lines represent simulation results using Eq. (1) due to annihilation only (dotted), repulsion only (dashed) and their combination (solid). (b) Simulated relative increase of $\Delta\,\mathrm{PL} = [\mathrm{PL}(t) - \mathrm{PL}(0)]/\mathrm{PL}_{\max}$; scale bar is $1\,\mu$m. (c) Spatially-dependent time $\tau_{\max}$ for the PL to reach its maximum, extracted from measurements and simulation using best fit $U_0 = 1.7 \times 10^{-15}\,\mathrm{eV\,cm}^2$. (d) Measured density-dependence of the PL decay time and relative yield, corresponding to the exciton-exciton annihilation coefficient $R_A = 5 \times 10^{-3}\,\mathrm{cm}^2/\mathrm{s}$.

tected by extracting either differential spatial profiles at different times or PL transients at different positions. For example, the delay time $\tau_{\max}$ of the maximum PL intensity rises with the increasing distance from the excitation spot in case of repulsion, as illustrated in Fig. 3 (b).

The results of this analysis are presented in Fig. 3 (c), demonstrating a characteristic feature of repulsion and determining the interaction constant $U_0 = 1.7 \times 10^{-15}\,\mathrm{eV\,cm}^2$ (see SM for detailed discussion). This interaction constant accounts for about one half of the observed increase of the effective diffusivity with excitation density. It is accompanied by a decrease of the PL lifetime and relative yield (Fig. 3 (c)), that are characteristic features of an efficient annihilation process with $R_A = 5 \times 10^{-3}\,\mathrm{cm}^2/\mathrm{s}$. Consequently, both annihilation and repulsion are found to contribute to the non-linear propoagation of IXs in roughly equal measures; the corresponding simulated result is shown in Figs. 2 (b) and 3 (a).

In general, regardless of the origin of the density dependent process, one typically finds sub-diffusive behavior of the mean-squared-displacement [24, 27, 32–34, 50]. It involves rapid initial diffusion that decreases towards smaller values at later times. Interestingly, it is not the case for the studied high-density conditions in the vicinity of the Mott transition. This is demonstrated by the normalized space- and time-resolved PL image in Fig. 4 (a) and the extracted $\Delta\sigma^2$ values in Fig. 4 (b) (upper panel). The data shows a rapid initial expansion during the first 50 ps followed by a contraction over several 100's of ps. This corresponds to an effective diffusion coefficient starting from $35\,\mathrm{cm}^2/\mathrm{s}$ and then decreasing to a *negative* value of $-5\,\mathrm{cm}^2/\mathrm{s}$, see upper panel of Fig. 4 (c). At later times, the contraction slows down and the effective diffusion coefficient increases again.

The effectively negative diffusivity of IXs is a consistent observation in the studied heterobilayer (see SM), albeit a highly unusual one. This implies a substantial change in the dynamics of the optically exited electron-hole pairs associated with the Mott transition. While a contraction of a quasiparticle cloud can be related to density-induced many-particle states such as droplet formation (see SM), interplay of multiple types of propagating, transient excitations is often a more likely cause [51–53]. At the studied density conditions close to the Mott threshold, a possible scenario would involve rapid propagation of short-lived plasma, followed by a slower diffusion of a small fraction of long-lived excitons. As schematically shown in Fig. 4 (d), this would effectively lead to a substantial broadening of the electron-hole distribution and a subsequent shrinking after the plasma recombines.

To illustrate the consequence of such a scenario, we use a simplified model with two components that both diffuse according to Eq. (1) (see SM for details). The resulting, simulated $\Delta\sigma^2$ and extracted, time-dependent diffusivity are presented in the lower panels of Fig. 4 (b) and (c), respectively. The analysis shows, that a two-component diffusion involving plasma and excitons could indeed lead

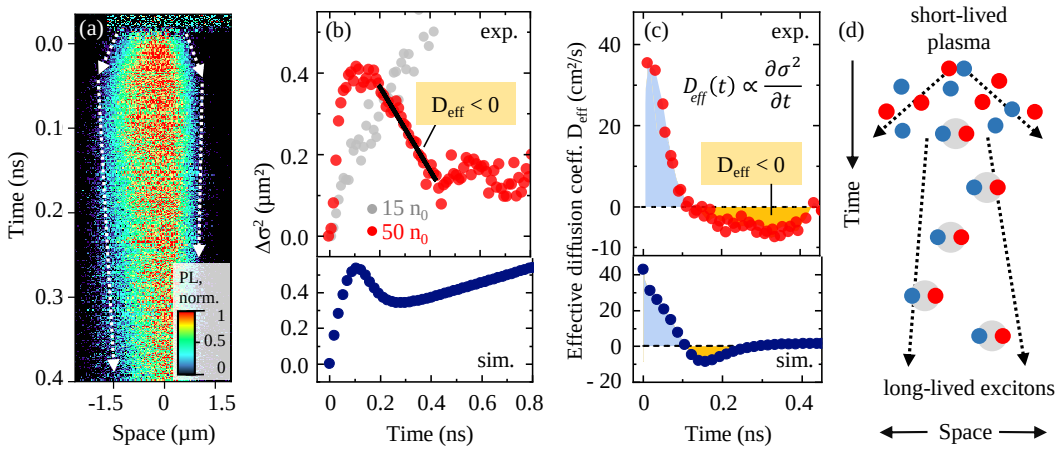

FIG. 4. (a) Streak camera image of the spatially- and time-resolved PL at T = 5 K in the high-density regime of about $6 \times 10^{12}\,\mathrm{cm}^{-2}$ ($50\,n_0$, pump energy density: $25\,\mu\mathrm{J\,cm}^{-2}$) above the Mott transition; the PL intensity is normalized at each time step. (b) (upper panel) Time-resolved mean squared displacement in experiment comparing high ($50\,n_0$) and intermediate ($15\,n_0$) densities. (lower panel) Simulation results showing the implications of a generic two-component model: rapidly expanding, short-lived plasma and longer-lived, slower excitons. (c) Corresponding time-dependent effective diffusion coefficients extracted from $D_{\mathrm{eff}} \propto \partial\sigma^2/\partial t$. (d) Schematic illustration of the two-component model.

to the observed behavior. We note, however, that an appropriate microscopic description of these intriguing findings involving a dense many-particle system above Mott threshold would be highly desirable.

In summary, we have shown that interlayer excitons in van der Waals heterostructures diffuse rapidly in the absence of moiré- and disorder-induced localization. Corresponding low-density diffusion coefficients are about 1000 times higher compared to those found in moiré superlattices, with temperature-dependent measurements confirming free diffusion. At elevated excitation densities we have demonstrated how the effects of exciton-exciton annihilation and repulsion can be distinguished and both provide substantial contributions to the non-linear propagation. Density range of the Mott transition revealed a highly unusual behavior involving rapid initial expansion followed by a long-lived effectively negative diffusion. Altogether, these findings should allow for disentanglement of complexities associated with dipolar excitons propagation in van der Waals heterostructures in both linear and non-linear regimes, demonstrating a promising platform for controllable exciton transport. The intriguing dynamics of electron-hole propagation at the exciton-plasma crossover should be of particular interest for a broad community studying physics of interacting electron-hole quasiparticles and correlated many-body states.

* alexey.chernikov@tu-dresden.de

[1] A. K. Geim and I. V. Grigorieva, Van der Waals heterostructures., Nature **499**, 419 (2013).

[2] K. S. Novoselov, A. Mishchenko, A. Carvalho, and A. H. Castro Neto, 2D materials and van der Waals heterostructures, Science **353**, 10.1126/science.aac9439 (2016).

[3] C. Jin, E. Y. Ma, O. Karni, E. C. Regan, F. Wang, and T. F. Heinz, Ultrafast dynamics in van der Waals heterostructures, Nature Nanotechnology **13**, 994 (2018).

[4] E. C. Regan, D. Wang, E. Y. Paik, Y. Zeng, L. Zhang, J. Zhu, A. H. MacDonald, H. Deng, and F. Wang, Emerging exciton physics in transition metal dichalcogenide heterobilayers, Nature Reviews Materials **7**, 778 (2022).

[5] H. Yu, G.-B. Liu, J. Tang, X. Xu, and W. Yao, Moiré excitons: From programmable quantum emitter arrays to spin-orbit–coupled artificial lattices, Science Advances **3**, e1701696 (2017).

[6] F. Wu, T. Lovorn, and A. H. MacDonald, Topological Exciton Bands in Moiré Heterojunctions, Physical Review Letters **118**, 147401 (2017).

[7] N. Zhang, A. Surrente, M. Baranowski, D. K. Maude, P. Gant, A. Castellanos-Gomez, and P. Plochocka, Moiré Intralayer Excitons in a $MoSe_2/MoS_2$ Heterostructure, Nano Letters **18**, 7651 (2018).

[8] C. Jin, E. C. Regan, A. Yan, M. Iqbal Bakti Utama, D. Wang, S. Zhao, Y. Qin, S. Yang, Z. Zheng, S. Shi, K. Watanabe, T. Taniguchi, S. Tongay, A. Zettl, and F. Wang, Observation of moiré excitons in WSe_2/WS_2 heterostructure superlattices, Nature **567**, 76 (2019).

[9] K. L. Seyler, P. Rivera, H. Yu, N. P. Wilson, E. L. Ray, D. G. Mandrus, J. Yan, W. Yao, and X. Xu, Signatures of moiré-trapped valley excitons in $MoSe_2/WSe_2$ heterobilayers, Nature **567**, 66 (2019).

[10] E. M. Alexeev, D. A. Ruiz-Tijerina, M. Danovich, M. J. Hamer, D. J. Terry, P. K. Nayak, S. Ahn, S. Pak, J. Lee, J. I. Sohn, M. R. Molas, M. Koperski, K. Watanabe, T. Taniguchi, K. S. Novoselov, R. V. Gorbachev, H. S. Shin, V. I. Fal'ko, and A. I. Tartakovskii, Resonantly hybridized excitons in moiré superlattices in van der Waals heterostructures, Nature **567**, 81 (2019).

[11] K. Tran, G. Moody, F. Wu, X. Lu, J. Choi, K. Kim, A. Rai, D. A. Sanchez, J. Quan, A. Singh, J. Embley, A. Zepeda, M. Campbell, T. Autry, T. Taniguchi,

K. Watanabe, N. Lu, S. K. Banerjee, K. L. Silverman, S. Kim, E. Tutuc, L. Yang, A. H. MacDonald, and X. Li, Evidence for moiré excitons in van der Waals heterostructures, Nature **567**, 71 (2019).

[12] Y. Xu, S. Liu, D. A. Rhodes, K. Watanabe, T. Taniguchi, J. Hone, V. Elser, K. F. Mak, and J. Shan, Correlated insulating states at fractional fillings of moiré superlattices, Nature **587**, 214 (2020).

[13] E. C. Regan, D. Wang, C. Jin, M. I. Bakti Utama, B. Gao, X. Wei, S. Zhao, W. Zhao, Z. Zhang, K. Yumigeta, M. Blei, J. D. Carlström, K. Watanabe, T. Taniguchi, S. Tongay, M. Crommie, A. Zettl, and F. Wang, Mott and generalized Wigner crystal states in WSe_2/WS_2 moiré superlattices, Nature **579**, 359 (2020).

[14] Y. Tang, L. Li, T. Li, Y. Xu, S. Liu, K. Barmak, K. Watanabe, T. Taniguchi, A. H. MacDonald, J. Shan, and K. F. Mak, Simulation of Hubbard model physics in WSe_2/WS_2 moiré superlattices, Nature **579**, 353 (2020).

[15] P. Merkl, F. Mooshammer, P. Steinleitner, A. Girnghuber, K.-Q. Lin, P. Nagler, J. Holler, C. Schüller, J. M. Lupton, T. Korn, S. Ovesen, S. Brem, E. Malic, and R. Huber, Ultrafast transition between exciton phases in van der Waals heterostructures, Nature Materials **18**, 691 (2019).

[16] L. V. Butov, A. Zrenner, G. Abstreiter, G. Böhm, and G. Weimann, Condensation of Indirect Excitons in Coupled AlAs/GaAs Quantum Wells, Physical Review Letters **73**, 304 (1994).

[17] R. Rapaport, G. Chen, D. Snoke, S. H. Simon, L. Pfeiffer, K. West, Y. Liu, and S. Denev, Charge Separation of Dense Two-Dimensional Electron-Hole Gases: Mechanism for Exciton Ring Pattern Formation, Physical Review Letters **92**, 117405 (2004).

[18] P. Rivera, J. R. Schaibley, A. M. Jones, J. S. Ross, S. Wu, G. Aivazian, P. Klement, K. Seyler, G. Clark, N. J. Ghimire, J. Yan, D. G. Mandrus, W. Yao, and X. Xu, Observation of long-lived interlayer excitons in monolayer $MoSe_2$–WSe_2 heterostructures, Nature Communications **6**, 6242 (2015).

[19] D. Unuchek, A. Ciarrocchi, A. Avsar, K. Watanabe, T. Taniguchi, and A. Kis, Room-temperature electrical control of exciton flux in a van der Waals heterostructure, Nature **560**, 340 (2018).

[20] P. Rivera, K. L. Seyler, H. Yu, J. R. Schaibley, J. Yan, D. G. Mandrus, W. Yao, and X. Xu, Valley-polarized exciton dynamics in a 2D semiconductor heterostructure, Science **351**, 688 (2016).

[21] J. Wang, Y. Guo, Y. Huang, H. Luo, X. Zhou, C. Gu, and B. Liu, Diffusion dynamics of valley excitons by transient grating spectroscopy in monolayer WSe_2, Applied Physics Letters **115**, 131902 (2019).

[22] E. V. Calman, M. M. Fogler, L. V. Butov, S. Hu, A. Mishchenko, and A. K. Geim, Indirect excitons in van der Waals heterostructures at room temperature, Nature Communications **9**, 1895 (2018).

[23] L. A. Jauregui, A. Y. Joe, K. Pistunova, D. S. Wild, A. A. High, Y. Zhou, G. Scuri, K. De Greve, A. Sushko, C.-H. Yu, T. Taniguchi, K. Watanabe, D. J. Needleman, M. D. Lukin, H. Park, and P. Kim, Electrical control of interlayer exciton dynamics in atomically thin heterostructures, Science **366**, 870 (2019).

[24] L. Yuan, B. Zheng, J. Kunstmann, T. Brumme, A. B. Kuc, C. Ma, S. Deng, D. Blach, A. Pan, and L. Huang, Twist-angle-dependent interlayer exciton diffusion in WS_2–WSe_2 heterobilayers, Nature Materials **19**, 617 (2020).

[25] J. Choi, W.-T. Hsu, L.-S. Lu, L. Sun, H.-Y. Cheng, M.-H. Lee, J. Quan, K. Tran, C.-Y. Wang, M. Staab, K. Jones, T. Taniguchi, K. Watanabe, M.-W. Chu, S. Gwo, S. Kim, C.-K. Shih, X. Li, and W.-H. Chang, Moiré potential impedes interlayer exciton diffusion in van der Waals heterostructures, Science Advances **6**, 10.1126/sciadv.aba8866 (2020).

[26] Z. Li, X. Lu, D. F. Cordovilla Leon, Z. Lyu, H. Xie, J. Hou, Y. Lu, X. Guo, A. Kaczmarek, T. Taniguchi, K. Watanabe, L. Zhao, L. Yang, and P. B. Deotare, Interlayer Exciton Transport in $MoSe_2/WSe_2$ Heterostructures, ACS Nano **15**, 1539 (2021).

[27] J. Wang, Q. Shi, E. M. Shih, L. Zhou, W. Wu, Y. Bai, D. Rhodes, K. Barmak, J. Hone, C. R. Dean, and X. Y. Zhu, Diffusivity Reveals Three Distinct Phases of Interlayer Excitons in $MoSe_2/WSe_2$ Heterobilayers, Physical Review Letters **126**, 1 (2021).

[28] Z. Sun, A. Ciarrocchi, F. Tagarelli, J. F. Gonzalez Marin, K. Watanabe, T. Taniguchi, and A. Kis, Excitonic transport driven by repulsive dipolar interaction in a van der Waals heterostructure, Nature Photonics **16**, 79 (2022).

[29] A. Raja, L. Waldecker, J. Zipfel, Y. Cho, S. Brem, J. D. Ziegler, M. Kulig, T. Taniguchi, K. Watanabe, E. Malic, T. F. Heinz, T. C. Berkelbach, and A. Chernikov, Dielectric disorder in two-dimensional materials, Nature Nanotechnology **14**, 832 (2019).

[30] Z. Vörös, R. Balili, D. W. Snoke, L. Pfeiffer, and K. West, Long-Distance Diffusion of Excitons in Double Quantum Well Structures, Physical Review Letters **94**, 226401 (2005).

[31] M. Stern, V. Garmider, E. Segre, M. Rappaport, V. Umansky, Y. Levinson, and I. Bar-Joseph, Photoluminescence Ring Formation in Coupled Quantum Wells: Excitonic Versus Ambipolar Diffusion, Physical Review Letters **101**, 257402 (2008).

[32] M. Kulig, J. Zipfel, P. Nagler, S. Blanter, C. Schüller, T. Korn, N. Paradiso, M. M. Glazov, and A. Chernikov, Exciton Diffusion and Halo Effects in Monolayer Semiconductors, Physical Review Letters **120**, 207401 (2018).

[33] A. J. Goodman, D.-H. Lien, G. H. Ahn, L. L. Spiegel, M. Amani, A. P. Willard, A. Javey, and W. A. Tisdale, Substrate-Dependent Exciton Diffusion and Annihilation in Chemically Treated MoS_2 and WS_2, The Journal of Physical Chemistry C **124**, 12175 (2020).

[34] J. Choi, J. Embley, D. D. Blach, R. Perea-Causín, D. Erkensten, D. S. Kim, L. Yuan, W. Y. Yoon, T. Taniguchi, K. Watanabe, K. Ueno, E. Tutuc, S. Brem, E. Malic, X. Li, and L. Huang, Fermi Pressure and Coulomb Repulsion Driven Rapid Hot Plasma Expansion in a van der Waals Heterostructure, Nano Letters **23**, 4399 (2023).

[35] M. Förg, L. Colombier, R. K. Patel, J. Lindlau, A. D. Mohite, H. Yamaguchi, M. M. Glazov, D. Hunger, and A. Högele, Cavity-control of interlayer excitons in van der Waals heterostructures, Nature Communications **10**, 3697 (2019).

[36] A. Weston, Y. Zou, V. Enaldiev, A. Summerfield, N. Clark, V. Zólyomi, A. Graham, C. Yelgel, S. Magorrian, M. Zhou, J. Zultak, D. Hopkinson, A. Barinov, T. H. Bointon, A. Kretinin, N. R. Wilson, P. H. Beton, V. I. Fal'ko, S. J. Haigh, and R. Gorbachev, Atomic reconstruction in twisted bilayers of transition metal

dichalcogenides, Nature Nanotechnology **15**, 592 (2020).
[37] M. R. Rosenberger, H.-J. Chuang, M. Phillips, V. P. Oleshko, K. M. McCreary, S. V. Sivaram, C. S. Hellberg, and B. T. Jonker, Twist Angle-Dependent Atomic Reconstruction and Moiré Patterns in Transition Metal Dichalcogenide Heterostructures, ACS Nano **14**, 4550 (2020).
[38] S. Zhao, Z. Li, X. Huang, A. Rupp, J. Göser, I. A. Vovk, S. Y. Kruchinin, K. Watanabe, T. Taniguchi, I. Bilgin, A. S. Baimuratov, and A. Högele, Excitons in mesoscopically reconstructed moiré heterostructures, Nature Nanotechnology 10.1038/s41565-023-01356-9 (2023).
[39] A. Castellanos-Gomez, M. Buscema, R. Molenaar, V. Singh, L. Janssen, H. S. J. van der Zant, and G. A. Steele, Deterministic transfer of two-dimensional materials by all-dry viscoelastic stamping, 2D Materials **1**, 011002 (2014).
[40] K. Wagner, E. Wietek, J. D. Ziegler, M. A. Semina, T. Taniguchi, K. Watanabe, J. Zipfel, M. M. Glazov, and A. Chernikov, Autoionization and Dressing of Excited Excitons by Free Carriers in Monolayer WSe_2, Physical Review Letters **125**, 267401 (2020).
[41] E. Barré, O. Karni, E. Liu, A. L. O'Beirne, X. Chen, H. B. Ribeiro, L. Yu, B. Kim, K. Watanabe, T. Taniguchi, K. Barmak, C. H. Lui, S. Refaely-Abramson, F. H. da Jornada, and T. F. Heinz, Optical absorption of interlayer excitons in transition-metal dichalcogenide heterostructures, Science **376**, 406 (2022).
[42] M. Brotons-Gisbert, H. Baek, A. Campbell, K. Watanabe, T. Taniguchi, and B. D. Gerardot, Moiré-Trapped Interlayer Trions in a Charge-Tunable $WSe_2/MoSe_2$ Heterobilayer, Physical Review X **11**, 031033 (2021).
[43] E. Liu, E. Barré, J. van Baren, M. Wilson, T. Taniguchi, K. Watanabe, Y.-T. Cui, N. M. Gabor, T. F. Heinz, Y.-C. Chang, and C. H. Lui, Signatures of moiré trions in $WSe_2/MoSe_2$ heterobilayers, Nature **594**, 46 (2021).
[44] X. Wang, J. Zhu, K. L. Seyler, P. Rivera, H. Zheng, Y. Wang, M. He, T. Taniguchi, K. Watanabe, J. Yan, D. G. Mandrus, D. R. Gamelin, W. Yao, and X. Xu, Moiré trions in $MoSe_2/WSe_2$ heterobilayers, Nature Nanotechnology **16**, 1208 (2021).
[45] P. E. Faria Junior and J. Fabian, Signatures of Electric Field and Layer Separation Effects on the Spin-Valley Physics of $MoSe_2/WSe_2$ Heterobilayers: From Energy Bands to Dipolar Excitons, Nanomaterials **13**, 1187 (2023).
[46] K. Wagner, J. Zipfel, R. Rosati, E. Wietek, J. D. Ziegler, S. Brem, R. Perea-Causín, T. Taniguchi, K. Watanabe, M. M. Glazov, E. Malic, and A. Chernikov, Nonclassical Exciton Diffusion in Monolayer WSe_2, Physical Review Letters **127**, 076801 (2021).
[47] J. Zipfel, M. Kulig, R. Perea-Causín, S. Brem, J. D. Ziegler, R. Rosati, T. Taniguchi, K. Watanabe, M. M. Glazov, E. Malic, and A. Chernikov, Exciton diffusion in monolayer semiconductors with suppressed disorder, Physical Review B **101**, 115430 (2020).
[48] A. Steinhoff, M. Florian, M. Rösner, G. Schönhoff, T. O. Wehling, and F. Jahnke, Exciton fission in monolayer transition metal dichalcogenide semiconductors, Nature Communications **8**, 1166 (2017).
[49] R. Rapaport, G. Chen, and S. H. Simon, Nonlinear dynamics of a dense two-dimensional dipolar exciton gas, Physical Review B **73**, 033319 (2006).
[50] N. S. Ginsberg and W. A. Tisdale, Spatially Resolved Photogenerated Exciton and Charge Transport in Emerging Semiconductors, Annual Review of Physical Chemistry **71**, 1 (2020).
[51] R. Rosati, K. Wagner, S. Brem, R. Perea-Causín, E. Wietek, J. Zipfel, J. D. Ziegler, M. Selig, T. Taniguchi, K. Watanabe, A. Knorr, A. Chernikov, and E. Malic, Temporal Evolution of Low-Temperature Phonon Sidebands in Transition Metal Dichalcogenides, ACS Photonics **7**, 2756 (2020).
[52] J. D. Ziegler, J. Zipfel, B. Meisinger, M. Menahem, X. Zhu, T. Taniguchi, K. Watanabe, O. Yaffe, D. A. Egger, and A. Chernikov, Fast and Anomalous Exciton Diffusion in Two-Dimensional Hybrid Perovskites, Nano Letters **20**, 6674 (2020).
[53] D. Beret, L. Ren, C. Robert, L. Foussat, P. Renucci, D. Lagarde, A. Balocchi, T. Amand, B. Urbaszek, K. Watanabe, T. Taniguchi, X. Marie, and L. Lombez, Nonlinear diffusion of negatively charged excitons in monolayer WSe2, Physical Review B **107**, 045420 (2023).

ACKNOWLEDGMENTS

We thank Sivan Refaely-Abramson, Andreas Beer, Jonas Zipfel, and Archana Raja for helpful discussions, as well as Imke Gronwald, Christian Bäuml, and Nicola Paradiso for their assistance with pre-patterned substrate preparation. Financial support by the DFG via SPP2244 (Project-ID: 443405595), Emmy Noether Initiative (CH 1672/1, Project-ID: 287022282), SFB 1277 (project B05), the Würzburg-Dresden Cluster of Excellence on Complexity and Topology in Quantum Matter (ct.qmat) (EXC 2147, Project-ID 390858490) and the Munich Center for Quantum Science and Technology (MCQST) (EXC 2111, Project-ID 390814868) is gratefully acknowledged. A. H. acknowledges funding by the European Research Council (ERC) (Grant Agreement No. 772195). K.W. and T.T. acknowledge support from the JSPS KAKENHI (Grant Numbers 20H00354, 21H05233 and 23H02052) and World Premier International Research Center Initiative (WPI), MEXT, Japan. A. S. and M. F. would like to acknowledge resources for computational time at the HLRN (Göttingen/Berlin). M. F. acknowledges support by the Alexander von Humboldt Foundation.